# Pressure Distribution Prediction for Two-Dimensional Hydrofoils with Massive Turbulent Separation

C.L.S. Farn,* F.R. Goldschmied,† and D.K. Whirlow‡
*Westinghouse Electric Corp., Pittsburgh, Pa.*

**An automated numerical algorithm has been developed for the prediction of the pressure distribution on two-dimensional noncavitating lifting hydrofoils, isolated or in cascade, even with massive turbulent flow separation. The only required inputs are the hydrofoil profile, the inlet flow angle, the cascade parameters, and the Reynolds Number. Satisfactory experimental verification of the algorithm has been achieved against the NACA 63-018 airfoil at 18° angle of attack, the NACA 65, 2-421 airfoil of 20° angle of attack, and the NASA GA(W)-1 airfoil at 21° angle of attack with turbulent separation locations up to 85% chord upstream of the trailing-edge. Only two iterations were required in the previous cases with a maximum computing time of 205 sec on the CDC 7600 system.**

## Nomenclature

$c$ = chord
$C_f$ = skin friction coefficient ($F/\frac{1}{2}\rho_i V_i^2 c$)
$C_{fo}$ = skin friction coefficient at start of turbulent adverse pressure gradient
$C_L$ = lift coefficient ($L/\frac{1}{2}\rho_i V_i^2 c$)
$C_p$ = static pressure coefficient [ $(P-P_i)/\frac{1}{2}\rho_i V_i^2 c$ ]
$C_{ps}$ = maximum pressure recovery coefficient at turbulent separation
$F$ = skin friction per unit span
$H$ = shape factor of the boundary layer = displacement thickness/momentum thickness
$JMAX$ = total number of node points (circles in Fig. 1)
$JSEP$ = total number of line segments on the separated portion of the blade surface (see Fig. 1)
$KMAX$ = total number of line segments on the entire blade surface (Fig. 1)
$L$ = lift per unit span
$n$ = unit vector normal to the surface of the body and pointing outward
$p$ = pressure
$Re$ = Reynolds number based on the chord and inlet flow conditions
$V$ = magnitude of velocity of the inviscid flow
$\boldsymbol{V}$ = velocity vector of the inviscid flow
$VX$ = $x$-component of $\boldsymbol{V}$
$VY$ = $y$-component of $\boldsymbol{V}$
$x$ = axis in the axial direction (Fig. 1)
$X$ = single airfoil chordwise length
$y$ = axis in the tangential direction (Fig. 1)
$y$ = axis in the tangential direction (Fig. 1)
$z$ = axis in the chord direction (Fig. 1)
$X_s$ = chordwise separation location

*Greek Symbols*§

$\alpha$ = angle of the uniform stream basic flow
$\beta$ = angle of the combined inviscid flow
$\gamma$ = angle formed by the tangent to the bare or modified blade contour and the $x$-axis
$\Gamma$ = strength of the strip vortex
$\delta$ = pitch to chord ratio
$\theta$ = momentum thickness of the boundary layer
$\lambda$ = strength of local blowing
$\nu$ = fluid kinematic viscosity
$\xi$ = stagger angle (Fig. 1)
$\rho$ = density
$\phi$ = velocity potential

*Subscripts*

$0$ = of the 0-degree uniform stream basic flow
$90$ = of the 90-degree uniform stream basic flow
$b$ = of the blowing flow on the blade surface
$i$ = upstream of the cascade or airfoil
$s$ = of the strip vortex basic flow

Received Oct. 27, 1975; revision received Feb. 18, 1976. Work funded under Westinghouse corporate research program.
Index Categories: Hydrodynamics; Marine Hydrodynamics, Vessel and Control Surface; Aircraft Aerodynamics.
*Fellow Engineer, Research Laboratories.
†Advisory Scientist, Research Laboratories. Associate Fellow, AIAA.
‡Manager, Fluid Dynamics, Research Laboratories.
§All of the angles defined here are measured with respect to the $x$-axis, and are considered to be positive if counterclockwise.

## I. Introduction

A classic hydrodynamic problem is the theoretical prediction of the pressure distribution on two-dimensional lifting hydrofoils, isolated or in cascade, given only the geometrical foil profile, the angle of attack or inlet flow angle, the cascade parameters, and the Reynolds number. If flow separation is absent, the solution to this problem is well known. However, if massive flow separation is present, a solution to this problem is not yet generally recognized. Indeed, in the 37th Wright Brothers Lecture[1] (1975), A.M.O. Smith classifies the prediction of the maximum lift coefficient as a problem beyond the present state-of-the-art.

Flow separation may be either laminar or turbulent, and the separated flow may or may not reattach downstream. Also transition from laminar to turbulent flow may occur before laminar separation, or it may occur in the separation bubble before reattachment. McCullough and Gault[2] (1951) have presented an extensive experimental study for a series of five airfoil sections in regard to airfoil stall; stall has been classified in the following three categories:

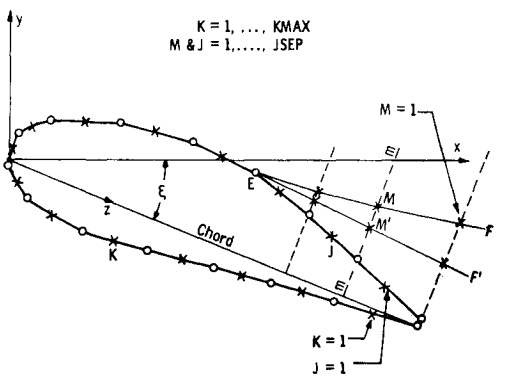


**Fig. 1 Schematic diagram of modified-body model.**

*a*) *Trailing-edge stall:* turbulent flow separation moving gradually upstream from the trailing-edge as the angle of attack is increased. Laminar separation was either preceded by transition, (i.e., laminar separation did not occur) or was followed by quick turbulent reattachment (short bubble with transition).

*b*) *Leading-edge stall:* laminar-flow separation near the leading-edge without any reattachment.

*c*) *Thin-airfoil stall:* laminar-flow separation near the leading-edge, with flow reattachment (long bubble) at a point which moves progressively downstream as the angle of attack is increased.

The present paper is concerned only with the first case of turbulent-flow separation because of the difficulties of dealing with long laminar separation bubbles, although the algorithm would still be applicable if a good model of the laminar bubble dynamics were available. The method is based on the iterative application of an inviscid theory and a boundary-layer theory, until convergence is achieved.

Then a correction is applied to the pressure level of the constant-pressure separation region, according to an empirical aerodynamic correlation of separation pressure against separation location. The following mathematical models are included in the algorithm assembly: a) Improved inviscid cascade flow model, where a separation location is assigned on the hydrofoil, and constant pressure is maintained downstream. b) Keller/Cebeci[3] laminar and turbulent boundary-layer algorithm. c) Michel/Smith[4] laminar/turbulent transition criterion. d) Modified Goradia/Lyman[5] laminar stall criterion. e) Goldschmied[6] criterion for maximum pressure recovery with turbulent flow separation (using Keller/Cebeci initial skin-friction coefficient values). f) Correlation of turbulent separation pressure levels against chordwise separation location on hydrofoil or airfoil.

Part II of the paper deals with the inviscid method, Part III presents the boundary-layer methods, and Part IV sets forth the experimental verification.

## II. Separated Inviscid Flow Model

A velocity potential exists for irrotational motion of an incompressible fluid and satisfies the Laplace equation

$$\nabla^2\phi = 0 \tag{1}$$

The velocity potential $\phi$ is related to the velocity vector $V$ by:

$$V = \nabla\phi \tag{2}$$

For all flow problems without suction or blowing, the velocity component normal to the surface of a solid body must vanish. Hence, we have

$$V \cdot n = 0 \tag{3}$$

Since Eq. (1) is linear, the velocity potential for any given problem may be obtained by linearly superposing the velocity potentials for basic flows. The superposed velocity potential must satisfy the boundary condition of Eq. (3), even though the component solutions need not. For two-dimensional plane flows, the basic flows are *source, vortex,* and *uniform stream.*

Figure 1 shows the contour of a given blade represented by a series of node points (circles). The adjacent node points are joined by straight line segments. The center points (crosses) of these segments are numbered by the integer $K$, which increases from 1 to $KMAX$ as one moves clockwise along the blade contour from the trailing edge. The cascade flow, which forms an angle $\alpha$ with respect to the $x$-axis is obtained by linearly superposing 0-deg and 90-deg uniform streams, a strip vortex of strength $\Gamma$ and their associated surface sources. Hence, the velocity at the $K$th center point becomes

$$V_K = (V_0)_K \cos\alpha + (V_{90})_K \sin\alpha + (V_s)_K \Gamma \tag{4}$$

$(V_0)_K$ is the velocity at the $K$th center point due to the unit 0-deg uniform stream and its associated surface source, which is so computed that Eq. (3) is satisfied on the *bare* blade surfaces for the unit 0-deg uniform stream. The variables $(V_{90})_K$ and $(V_s)_K$ in Eq. (4) are defined in a similar manner. The formulas for computing the variables $(V_0)_K$, $(V_{90})_K$, and $(V_s)_K$ were derived by Giesing[7] in 1964 under the U.S. Navy Fundamental Hydromechanics Research Program and will not be repeated in this paper.

The velocity and the flow angle upstream of the cascade are related to $\alpha$, $\Gamma$, and $\delta$ by the following equations,

$$V_i = (1 + 2T\sin\alpha + T^2)^{1/2} \tag{5}$$

$$\beta_i = \tan^{-1}[(\sin\alpha + T)/\cos\alpha] \tag{6}$$

where

$$T = \Gamma/2\delta \tag{7}$$

In the computation of cascade flows, the upstream angle $\beta_i$ and the pitch to chord ratio $\delta$ are always specified. Hence, Eq. (6) and the Kutta condition are used for determining $\alpha$ and $\Gamma$. Equation (6) also implies that the upstream flow angle $\beta_i$ is generally not equal to the angle $\alpha$ of the uniform stream used as one of the basic flows in the computation, unless $\delta \to \infty$ (i.e., single airfoil) or $\Gamma = 0$ (i.e., cascade of nonlifting bodies).

The blade surface velocity $V_K$ computed by Eqs. (4)-(6) is only valid for the attached cascade flows because the stagnation steamlines on both pressure and suction surfaces of the blade do not break away from them before reaching the trailing edge. For cascade flow with extensive turbulent separation, the flow does not follow the contour of the bare blade downstream of the separation point on the suction surface. In fact, it follows a self-formed contour called a separated streamline. Test data[2,8,9] indicate that, if turbulent separation occurs in a cascade (or a single airfoil) flow, the pressure distribution on the separated portion of the blade (or airfoil) surface is approximately uniform. This observation holds even if the separation region covers as much as 85% of the blade chord.

There are three models available for computing pressure distributions on the blade (or airfoil) surfaces for separated flows with assigned separation points. They will be denoted here as the separated streamline model, the bare-body model, and the modified-body model. They will be discussed in the rest of this section.

### A. Separated-Streamline Model

This model was initially developed by Jacob,[10] and then adopted by Abbott.[11] It was also used by Hahn, Rubbert, and Mahal.[12] It is based on the assumption that the pressure in the separation region above the airfoil is uniform. The separation region is mathematically simulated by blowing along the separated portion (*ABC* in Fig. 2) of the airfoil surface. The distribution of the local blowing strength $\lambda$ is determined empirically.

On the separated portion of the airfoil surface, (*ABC* in Fig. 2), the velocity is not computed; instead, it is assumed equal to the velocity at the separation point $A$. This assumption, of course, is consistent with the basic assumption of this model, that the pressure in the separated region above the airfoil is uniform. Unfortunately, the numerical results of Ref. 11 indicate the computed velocity (hence the pressure) along

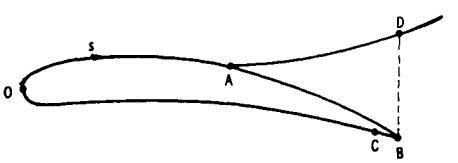


**Fig. 2 Schematic diagram of separated-streamline model.**

the separated streamline ($AD$ in Fig. 2) is far from being uniform. This implies that the empirically determined distribution of $\lambda$ is not consistent with the basic assumption, at least, for the airfoil geometry studied in Ref. 11.

**B. Bare-Body Model**

This model was developed by Geller[13] in 1972 for the separated cascade flows. Referring to Fig. 1, the separated portion of the blade surface is represented by JSEP line segments. Geller *enforces the uniform pressure distribution* on the bare blade surface downstream of the separation point by mathematically manipulating the local blowing strength. Geller showed this model yielded correct pressure distributions for compressor cascade flows with small* turbulent separations. Nevertheless, the ability of this model to predict the correct pressure distributions for cascade flows with large turbulent separation remained in question.

**C. Modified-Body Model**

This model was developed during the course of the present research. In short, the blade contour is modified downstream of the separation point, such that the pressure distribution along the modified portion of the blade contour is uniform, and of course, the velocity is tangential to it. Referring to Fig. 1, curve $EF$ represents the modified contour of the blade. This curve is obtained by distributed blowing along the separated portion of the bare blade surface (i.e., on the line segments $J=1,2,\ldots,JSEP$) in the same manner as described in Sec. II-B. However, the strength of the blowing is determined by different conditions.

The velocity on the attached portion of the blade surface is computed by the following formula,

$$V_K=(V_0)_K\cos\alpha+(V_{90})_K\sin\alpha+(V_s)_K\Gamma+\sum_{J=1}^{JSEP}(V_b)_{KJ}\lambda_J \tag{8}$$

and the velocity on the separated portion of the blade surface is assumed to be equal to that on the modified blade contour $EF$. The parameters $\alpha$, $\Gamma$, and $\lambda_J$ in Eq. (8) are determined simultaneously by Eq. (6) and the following relations,

$$p_{K=1}=p_{K=(KMAX-JSEP)}=p_{M=1}=p_{M=2}=\ldots=p_{M=JSEP} \tag{9}$$

where the integer $M$ denotes the off-body points at the intersections of the straight lines $mm$ and the curve $EF$ (see Fig. 1). It is worth noting that each of the straight lines $mm$ passes a blade node point (not to be confused with the center point of the line segment) in the separation region, and is normal to the chord.

The shape of the modified blade contour $EF$ is obtained by iteration according to the following procedure. If the pressure is forced to be constant at the intersection points $M'$ (Fig. 1) of the straight lines $mm$ and a guessed curve (or a straight line) $EF'$ which approximates the true modified blade contour $EF$, the resultant flow angles $\beta_{M'}$ at these intersections are very close to the corresponding values of $\gamma_M$, computed according to the curve $EF$. It is important to note that although $EF'$ may approximate $EF$ in location, their local curvatures could be considerably different. Therefore $\gamma_{M'}$ is generally quite different from $\gamma_M$. Once the values of $\gamma_M$ are known, it is not difficult to construct the curve $EF$ starting from the separation point $E$. With this procedure, it was possible to find the modified blade contour $EF$ for almost all of the separated cascade flows investigated in this paper within four iterations. In most cases the separation regions cover as much as 50% of the chord, with a maximum of 85%.

*The largest separation region studied by Geller covers approximately 10% of the blade chord, as compared to 85% in the present work.

The criterion for the convergence on the location of $EF$ is as follows

$$|\beta_M-\gamma_M|<1^\circ \tag{10}$$

Theoretically, of course, $\beta_M$ should be equal to $\gamma_M$.

Since the pressure is not a direct dependent variable in potential flow theory, it is desirable to transform Eq. (9) into the following form,

$$V_{K=1}=V_{K=(KMAX-JSEP)}=V_{M=1}=V_{M=2}=\ldots=V_{M=JSEP} \tag{11}$$

As mentioned earlier, the integer $K$ denotes the center points of the line segments which approximate the bare blade surface and $M$, the points on the modified blade contour. Hence $V_K$ is the velocity at the on-body points, and can be computed directly by linearly superposing the 0-deg uniform stream, 90-deg uniform stream, strip vortex, and the distributed blowing on the separated portion of the blade surface as indicated by Eq. (8). The variable $V_M$ in Eq. (11) is the velocity at the off-body points, and only its $x$-component $VX_M$ and $y$-component $VY_M$ can be computed directly from the aforementioned basic flows. The formulas for computing $VX_M$ and $VY_M$ are given as follows

$$VX_M=(VX_0)_M\cos\alpha+(VX_{90})_M\sin\alpha+(VX_s)_M\Gamma+\sum_{J=1}^{JSEP}(VX_b)_{MJ}\lambda_J \tag{12a}$$

$$VY_M=(VY_0)_M\cos\alpha+(VY_{90})_M\sin\alpha+(VY_s)_M\Gamma+\sum_{J=1}^{JSEP}(VY_b)_{MJ}\lambda_J \tag{12b}$$

where $(VX_0)_M$ and $(VY_0)_M$ are the $x$- and $y$-components of velocity, respectively, at the off-body point $M$ due to the unit 0-deg uniform stream and its associated surface source. The variables $(VX_{90})_M$, $(VY_{90})_M$, $(VX_s)_M$ and $(VY_s)_M$ are defined in a similar manner. The variables $(VX_b)_{MJ}$ and $(VY_b)_{MJ}$ are the $x$- and $y$- component of velocity, respectively, at the off-body point $M$ due to the unit blowing on the $J$th segment on the separated portion of the blade (Fig. 1).

Since $V_M$ in Eq. (11) can not be computed by linearly superposing the basic flows, Eq. (11) must be further transformed into a workable form, that is

$$VX_M=V_E\cos\beta_M,\ \text{for } M=1,2,\ldots,JSEP \tag{13a}$$

$$VY_M=V_E\sin\beta_M,\ \text{for } M=1,2,\ldots,JSEP \tag{13b}$$

$$V_K=V_E,\ \text{for } K=1 \text{ and } (KMAX-JSEP) \tag{13c}$$

where $V_E$ is the velocity at the separation point $E$ (Fig. 1).

Substitution of Eqs. (12a) into (13a), (12b) into (13b), (8) into (13c) results, after some rearrangement, in the following equations

$$\sum_{j=1}^{JSEP}\left(\frac{\lambda_J}{\cos\alpha}\right)(VX_b)_{MJ}+(\tan\alpha)(VX_{90})_M+\left(\frac{\Gamma}{\cos\alpha}\right)(VX_s)_M-\left(\frac{V_E}{\cos\alpha}\right)\cos\beta_M=-(VX_0)_M,\ \text{for } M=1,2,\ldots,JSEP \tag{14a}$$

$$\sum_{j=1}^{JSEP}\left(\frac{\lambda_J}{\cos\alpha}\right)(VY_b)_{MJ}+(\tan\alpha)(VY_{90})_M+\left(\frac{\Gamma}{\cos\alpha}\right)(VY_s)_M-\left(\frac{V_E}{\cos\alpha}\right)\sin\beta_M=-(VY_0)_M,\ \text{for } M=1,2,\ldots,JSEP \tag{14b}$$

$$\sum_{J=1}^{JSEP}\left(\frac{\lambda_J}{\cos\alpha}\right)(V_b)_{KJ}+(\tan\alpha)(V_{90})_K+\left(\frac{\Gamma}{\cos\alpha}\right)$$

$$(V_s)_K-\left(\frac{V_E}{\cos\alpha}\right)=-(V_0)_K,\ \text{for } K=1 \text{ and } (KMAX-JSEP) \tag{14c}$$

Equations (14) and (6) add up to a total of $(2\times JSEP+3)$ independent equations which are necessary and sufficient to determine the parameters $\tan\alpha$, $\Gamma/\cos\alpha$, $V_E/\cos\alpha$, $\lambda_J/\cos\alpha$ and $\beta_M$ (Note: both $J$ and $M$ vary from 1 to $JSEP$). However, a unique real-value solution is not guaranteed because of the nonlinearity of the equations. Assuming a physically meaningful real-value solution exists, the task was to find a method which would consistently yield this solution. After many numerical experiments, two methods seem to be reasonably reliable. They are Newton-Raphson iteration[14] and Function Minimization.[15] The former method takes less computer time to obtain a convergent solution. However, the latter yields a somewhat better solution with respect to the experimental data. Therefore, the Function Minimization method was adopted. It is of interest to note that in Ref. 12 the numerical attempts were limited by the lack of an automated convergence procedure, and that this was recognized as the main objective of future work.

This Modified-Body model is used in the automated algorithm for all inviscid flow computations. The boundary-layer and wake displacement effects have not been considered yet in the pressure distribution computation.

## III. Boundary-Layer Methods

A numerical method is now needed for the computation of the steady-state two-dimensional incompressible boundary-layer with all of the associated phenomena. Three choices had to be made. The *first choice* was to adopt the Keller and Cebeci[3] method for the basic computation of the laminar and of the turbulent boundary layer. The *next choice* concerns laminar separation. Essentially three criteria are required: one for determining when transition precludes laminar separation, another for determining when the detached flow will not reattach to the surface, and a third for evaluating the extent of the laminar separation bubble and its associated momentum loss, i.e., the initial momentum thickness of the turbulent flow at the reattachment point.

Transition is assumed to follow the Michel and Smith criterion as outlined by Smith and Gamberoni[4] for low freestream turbulence or to follow the neutral stability criterion as given by Rosenhead[16] for high freestream turbulence. Transition is assumed to occur instantaneously and, if it occurs before laminar separation, then said separation is assumed to be avoided (first criterion). For the second criterion, a modified Lyman and Goradia[5] curve is used to determine the occurrence of flow reattachment or of permanent laminar stall. If laminar stall occurs, then the algorithm is stopped. If flow reattachment occurs, then the third criterion is needed to determine the initial location and initial values for the turbulent flow computation. This criterion is still absent in the present algorithm: transition is assumed to occur instantaneously at the separation point (zero bubble length) and the initial turbulent boundary-layer thickness is stepped to $R_\theta=450$ if the final laminar value is lesser. Other authors, such as Stevens, Goradia, and Braden[5] and Scruggs, Nash, and Singleton[17] follow similar procedures in their boundary-layer algorithm. Further research appears to be needed for the formulation of this important third criterion.

The *third choice* concerns the turbulent separation criterion to be employed. This criterion has to be both physically sound and tractable numerically within the algorithm framework. The classical turbulent separation criterion is the statement of zero skin-friction, which was derived mathematically for steady-state laminar separation and adopted by analogy for the turbulent case, although turbulent flow separation is never steady state in physical reality. The closed-loop characteristic of the present automated algorithm provides the theoretical basis for the understanding of the typical separated flow oscillatory behavior.

The embodiment of the criterion into a prediction method depends greatly on the following: a) selection of boundary-layer computational method; and b) pressure distribution employed for the previous method in the vicinity of separation. For instance, with the Keller and Cebeci boundary-layer method, if the *experimental pressure distribution* is used for any separated airfoil, the method will never predict zero skin-friction but only a skin-friction dip to a finite value, followed by an increase. Cebeci, Mosinskis, and Smith[18] recognize this and suggest that the experimental pressure distribution be "extrapolated" along some tangent before reaching the typical separation concavity (Figs. 2 and 3, Ref. 18), for use as input to their boundary-layer method. Then the authors locate the zero skin-friction point along the "extrapolated" line and transfer it up at the same chordwise position to the actual experimental pressure curve and mark it thereon. By this procedure, good results are shown in terms of chordwise separation prediction but the large errors in pressure-recovery prediction are ignored. Hahn, Rubbert, and Mahal[12] follow the same extrapolation procedure for the pressure distribution but the boundary-layer method is that used at the Boeing Airplane Company.[19] To illustrate the confusing aspects of this situation of "zero skin-friction," during the present research the NACA 63-018[2] airfoil was analyzed at 16° angle of attack, using the complete automated algorithm with the Keller and Cebeci boundary-layer method and *"zero skin-friction"* separation criterion. The separation prediction was at 73.5% chord (from the nose) while the experimental point was at 40.5% chord.

Hahn, Rubbert, and Mahal[12] analyzed the same NACA 63-018[2] airfoil at 16° angle of attack with their iterative algorithm, using the Boeing boundary-layer method and "zero skin-friction" separation criterion. Their separation prediction was at 50% chord. Thus, it should be abundantly clear that the simple statement of "zero skin-friction separation criterion" has little meaning unless it is accompanied by the specification of boundary-layer method and pressure extrapolation procedure.

After several trial runs with different airfoils with unsatisfactory results, it was decided to abandon the Keller and Cebeci zero skin-friction approach and to adopt the Goldschmied[6] criterion for the maximum pressure-recovery at separation, with the required initial skin-friction value computed by the Keller and Cebeci method despite the conclusions of Refs. 1 and 18.

This criterion is a simplified expression of the more comprehensive Townsend theory[26]. In both cases, the principal parameter is the ratio of maximum pressure recovery (at separation $C_{ps}$ over the turbulent skin-friction coefficient $C_{fo}$ at the start of the turbulent adverse pressure gradient. This initial turbulent point may be at the minimum pressure location or downstream. For the Goldschmied criterion this ratio is constant, regardless of the adverse pressure distribution history: $C_{ps}/C_{fo}=200$. It was clearly recognized by the author that this was but a convenient first approximation, with good validity in the range of most airfoil test data (Fig. 9 of Ref. 6). For the Townsend method, the ratio $C_{ps}/C_{fo}$ is a very complicated function of the initial velocity $U_0$, and of the pressure gradient "at separation." It is this last term which is very difficult to define experimentally, since it ranges down to zero as the pressure distribution flattens out at separation.

It must be well understood that the *Goldschmied criterion is not a prediction method by itself,* because it must be supplied the initial skin-friction value by a selected boundary-layer method. The only true test of the criterion can be achieved using experimental skin-friction values and experimental pressure recoveries. The combination of the Goldschmied

criterion with the Keller and Cebeci boundary-layer method will be not yield the same predictions as another combination such as that with the Ludwig-Tillman skin-friction or that with the Boeing skin-friction.

As an illustrative example, Goldschmied[6] analyzed the NACA 65(216)-222 airfoil (Data Set I, Ref. 6) at 10.1° angle of attack with the *Ludwig-Tillman skin-friction* and predicted a separation presure-recovery coefficient of 0.495 (−1% error). Also Hahn, Rubbert, and Mahal[12] used the Goldschmied criterion with the *Boeing skin-friction* on the same airfoil (Fig. 4, Ref. 12) and predicted a pressure-recovery coefficient of 0.64 (+28% error).

Finally Cebeci, Mosinskis, and Smith[18] used the Goldschmied criterion with the *Cebeci and Smith skin-friction* on the same airfoil (Fig. 9, Ref. 18) and predicted a pressure-recovery coefficient of 0.517(+3.5% error). Also it should be pointed out that Ref. 18 modified the original Goldschmied[6] criterion by "extrapolating" the starting point of the adverse turbulent pressure-gradient back to the minimum-pressure point even in the cases where it actually occurred somewhere downstream.

The description of turbulent separation comprises two parameters, i.e., chordwise location and corresponding static-pressure coefficient. From preliminary work with the algorithm on isolated airfoils, it was found that the separation location was predicted satisfactorily but that the pressure coefficient (as dictated by the separated inviscid model) was too low and not responsive to separation location (as seen in Fig. 3). An empirical correlation was compiled from test data of six NACA and NASA isolated airfoils, relating separation pressure coefficient to separation chordwise location, as shown in Fig. 3. A mean line, as shown dashed in the figure, was selected for use in the algorithm. The computed inviscid separation location is entered in the horizontal scale, and the corrected separation pressure coefficient is thus determined.

## IV. Experimental Verification

To gain experience in the use of the automated algorithm on the Westinghouse CDC 7600 computer system and to verify its prediction against known experimental results, application was made to three NACA/NASA airfoils of 17%, 18%, and 21% thickness at the maximum available angle of attack.

In Fig. 4 there is shown the NACA 63-018 airfoil of Ref. 2 (1951) at 18° angle of attack, with the static pressure coefficient $C_p$ plotted against the dimensionless chordwise location $x/c$. The full line indicates the theoretical prediction with the Goldschmied criterion and the separation pressure correction while the dashed line indicates the theoretical prediction with the zero skin-friction criterion and the separation pressure correction. It is seen that there is excellent agreement between the full line and the test data points for the lower surface of the airfoil, and good agreement for the upper surface.

The experimental separation point, as determined by the pressure slopes intersection as shown in the figure, occurs at

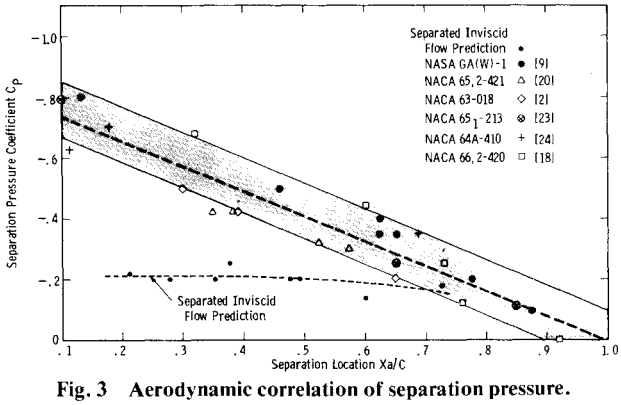


**Fig. 3 Aerodynamic correlation of separation pressure.**

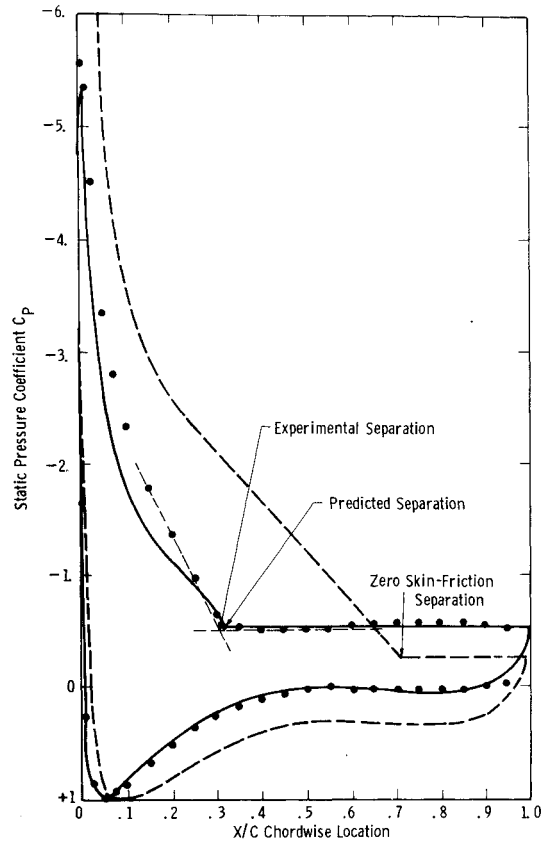


**Fig. 4 Comparison of theoretical (automated algorithm) airfoil pressure distribution and of experimental data for NACA 63-018 airfoil at 18° angle of attack.**

30.5% chord with a pressure coefficient of −0.52; the Goldschmied separation point occurs at 31.5% chord with a pressure coefficient of −0.54. The agreement is excellent, in terms of *both* location *and* pressure. On the other hand, the zero skin-friction separation point occurs at 71% with a pressure coefficient of −0.25; the agreement is bad, in terms of *both* location *and* pressure. For cavitation predictions it is required to consider the minimum pressure coefficient $C_{P\min}$. The experimental value is −7.05, with the Goldschmied prediction is −5.4, and the zero skin-friction prediction is −12.0. For a baseline reference, the inviscid attached flow at 18° has $C_{P\min} = -12.4$. In view of the close agreement of the separation point, the discrepancy in $C_{P\min}$ may be due to numerical difficulties in an area of extremely rapid change.

The 63-018 profile was given in Ref. 2; it was described numerically by 107 points, after obtaining poor results with only 55 points. The time on the CDC 7600 was 120 sec with 2 boundary-layer iterations for the computation with the Goldschmied criterion.

In Fig. 5 there is shown the NACA 65, 2-421 airfoil of Ref. 20 (1942) at 20.3° angle of attack, with the static pressure coefficient $C_P$ plotted against the dimensionless chordwise location $x/c$. The full line indicates the theoretical prediction with the Goldschmied criterion and the separation pressure correction while the dashed line indicates the theoretical prediction with the Goldschmied criterion and the separation correction while the dashed line indicates the theoretical prediction with the zero skin-friction criterion and the separation pressure correction. It is seen that there is good agreement between the full line and the test data points for the lower surface of the airfoil, while the agreement is only fair for the upper surface. One reason for this is certainly the fact that the airfoil profile was not given in Ref. 20 (1942) and that the profile input to the present algorithm was achieved by the numerical methods of Kinsey and Bowers[21], based on the 1945 aerodynamics formulation of Abbott, von Doenhoff,

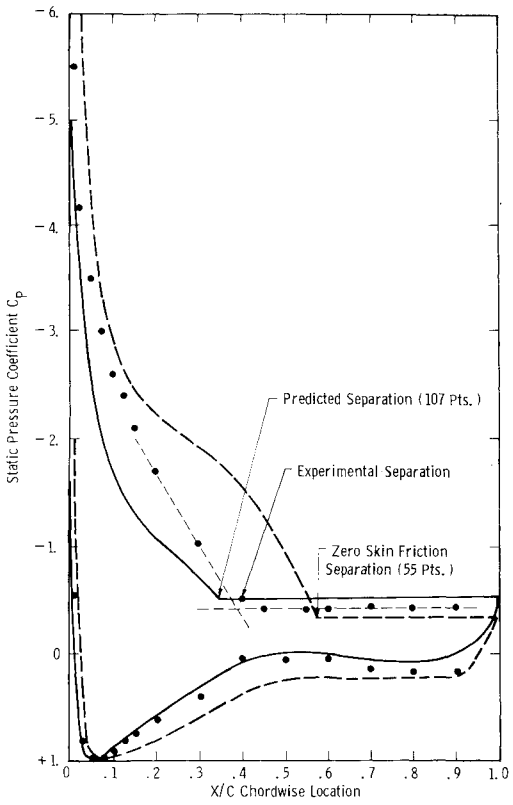


**Fig. 5 Comparison of theoretical (automated algorithm) airfoil pressure distribution and of experimental data for NACA 65, 2-421 airfoil at 20.3° angle of attack.**

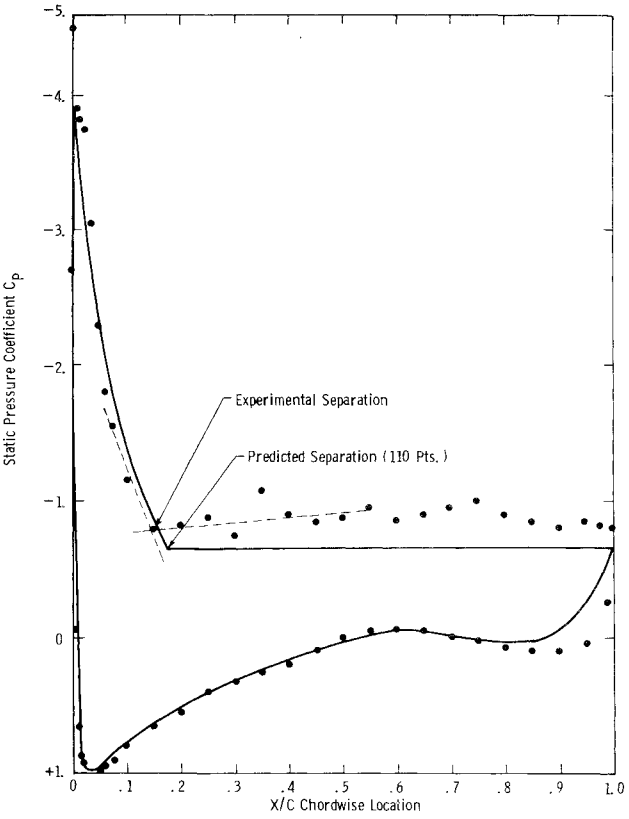


**Fig. 6 Comparison of theoretical (automated algorithm) airfoil pressure distribution and of experimental data for NASA GA(W)-1 airfoil at 21.14° angle of attack.**

and Stivers.[22] The experimental separation point, as determined by the pressure slopes intersection as shown in the figure, occurs at 39% chord with a pressure coefficient of −0.42. The Goldschmied separation point is predicted at 34% chord with a pressure coefficient of −0.52 with good agreement for location and fair agreement for pressure. On the other hand, the zero skin-friction separation point is predicted at 57.5% chord with a pressure coefficient of −0.34, with bad agreement for location and fair agreement for pressure. The experimental minimum pressure coefficient is −5.5, while the theoretical prediction is −5.0 for the Goldschmied criterion and −6.8 for the zero skin-friction criterion. For a baseline reference, the inviscid attached flow at 20.3° angle of attack has $C_{P\min} = -13.6$.

The Goldschmied computation was carried out with 107 profile points, requiring two boundary-layer iterations and 110 sec on the CDC 7600. With the zero skin-friction criterion and 107 points, the boundary-layer iterations exceeded the limitation of ten. The case was run with only 55 profile points requiring five boundary-layer iterations and 114 sec.

In Fig. 6 there is shown the NASA GA(W)-1 airfoil of Ref. 9 (1973) at 21.14° angle of attack, with the static pressure coefficients $C_P$ plotted against the dimensionless chordwise location $x/c$. The full line indicates the theoretical prediction with the Goldschmied criterion and the separation pressure correction. It is seen that there is excellent agreement on the lower surface of the airfoil and on the unseparated portion of the upper surface. The experimental separation point, as determined by the pressure slopes intersection as shown in the figure, occurs at 15% chord with a pressure coefficient of −0.80. The Goldschmied separation point is predicted at 17.5% chord with a pressure coefficient of −0.65. Considering that this airfoil is 85% under flow separation, the theoretical prediction may be deemed in excellent agreement for both location and pressure. The computation was carried out with 111 points and required two boundary-layer iterations and 205 sec on the CDC 7600. No computation was attempted in this case with the zero skin-friction criterion, in

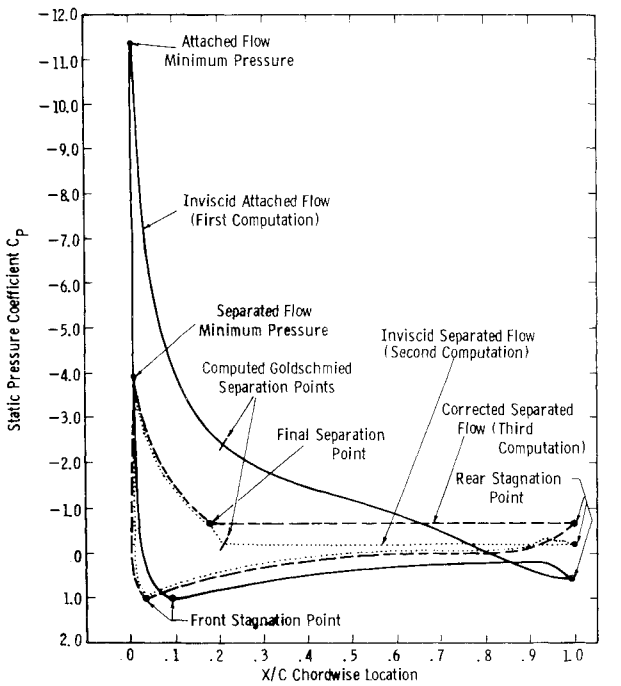


**Fig. 7 Iterative computation procedure for GA(W)-1@21° angle of attack.**

view of the experience of the previous airfoil. The experimental minimum pressure coefficient is −4.5 while the theoretical prediction is −3.9. For baseline reference, the inviscid attached flow at 21.14° has $C_{P\min} = -11.4$.

This case can also provide a good insight in the algorithm operation, if a pressure plot is made of the attached inviscid flow (first iteration), of the separated inviscid flow (second iteration) and of the final distribution with the separation pressure correction, as shown in Fig. 7. The front stagnation

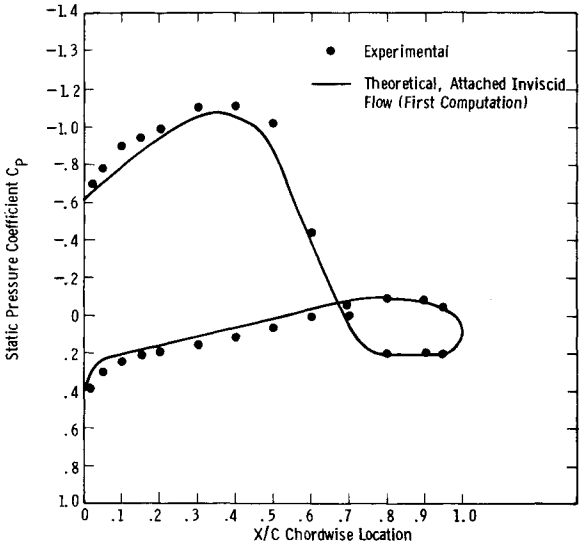


**Fig. 8 Comparison of theoretical (automated algorithm) airfoil pressure distribution and of experimental data for NACA 3-H-13.5 airfoil at 4.6° angle of attack.[25]**

and rear stagnation points are indicated, as well as the separation points computed according to the Goldschmied criterion for each iteration.

The interaction of viscous flow and inviscid flow is illustrated quite vividly in Fig. 7 by the large difference between the attached pressure distribution and the separated pressure distribution. Flow oscillations appear foreordained in such a closed-loop situation. Finally Fig. 8 shows the comparison between the theoretical pressure distribution and the experimental data for the NACA 3-H-13.5[25] airfoil at 4.6° angle of attack, with excellent agreement. At first glance the airfoil appears to be stalled, with separation location at 74% chord from the nose. Actually the flow is fully attached because a positive pressure ($C_p = 0.2$) occurs in the "separation" region. Indeed, the theoretical pressure shown in Fig. 8 is that for attached inviscid flow (first computation). Thus this airfoil provides an elegant test of the algorithm. The computing time was 2 sec on the CDC 7600.

## V. Conclusions

An automated algorithm has been assembled for the prediction of pressure distribution on two-dimensional noncavitating hydrofoils with massive turbulent flow separation. A successful experimental verification has been achieved on three airfoils, with separation location up to 85% chord upstream from the trailing-edge.

The hydrofoil profile must be described by a minimum of 100 points. Only two iterations were required in all three cases and the longest computing time was 205 sec on the CDC 7600 system.

Excellent agreement was achieved for the turbulent separation chordwise location and pressure coefficient with the Goldschmied criterion, but only fair agreement was obtained for the minimum pressure coefficient and therefore cavitation prediction. It is recommended that the following features be added to the algorithm:

a) Boundary-layer and wake displacement effects for the computation of the final pressure distribution. This would avoid the need for the separation pressure correction.

b) Laminar separation-bubble mechanism, to yield correct initial turbulent boundary-layer values.

It is suggested that the Townsend method be investigated within the framework of the algorithm, using the computed inviscid pressure gradient at the separation location as its separation gradient.

## References

[1] Smith, A.M.O., "High Lift Aerodynamics," *Journal of Aircraft*, Vol. 12, June 1975, pp. 501-530.

[2] McCullough, C.B. and Gault, D.E., "Examples of Three Representative Types of Airfoil-Section Stall at Low Speed," NACA TN-2502, 1951.

[3] Keller, H.B. and Cebeci, T., "Accurate Numerical Methods for Boundary Layer Flows-II. Two-Dimensional Turbulent Flows," AIAA Paper 71-164, 1971.

[4] Smith, S.M.O. and Gamberoni, N., "Transition Pressure Gradient and Stability Theory," Douglas Aircraft Co., Long Beach, Calif., Rept. ES 26388, 1956.

[5] Stevens, W.A., Goradia, S.H., and Braden, J.A., "Mathematical Model for Two-Dimensional Multi-Compoent Airfoils in Viscous Flow," NACA CR-1843, July 1971.

[6] Goldschmied, F.R., "An Approach to Turbulent Incompressible Separation Under Adverse Pressure Gradient," *Journal of Aircraft*, Vol. 2, March/April 1965, pp. 108-115.

[7] Giesing, J.P., "Extension of the Douglas Neumann Program to Problems of Lifting Infinite Cascades," Douglas Aircraft Co., Rept. LB31653, Long Beach, Calif., 1964.

[8] Herrig, L.J., Emery, J.C., and Erwin, J.R., "Systematic Two-Dimensional Cascade Tests of NACA 65-Series Compressor Blade at Low Speeds," NACA TN-3916, 1957.

[9] McGhee, R.J., "Low-speed Aerodynamic Characteristics of a 17% -Thick Airfoil Section Designed for General Aviation Applications," NASA TN D-7428, Dec. 1973.

[10] Jacob, K., "Berechnung der abgelösten inkompressiblen Strömung um Tragflügeprofile und Bestimmung des maximalen Auftriebs," *Z. Flugwiss*, Vol. 17, 1969, pp. 221-230.

[11] Abbott, D.E., "Prediction of Flows With and Without Partial Separation," Purdue University, Lafayette, Ind., Fluid Mechanics Group Report, 1972.

[12] Hahn, M., Rubbert, P.E. and Mahal, A.S., "Evaluation of Separation Criteria and Their Application to Separated Flow Analysis," Airforce Flight Dynamics Lab., Wright-Patterson AFB, Ohio, Technical Rept. AFFDL-TR-72-145 Air Force Systems Command, Jan. 1973.

[13] Geller, W., "Incompressible Flow Through Cascades with Separation," AGARDograph No. 164, 1972.

[14] Hildebrand, F.B., *Introduction to Numerical Analysis*, McGraw-Hill, N.Y., 1956, pp. 450-451.

[15] Fletcher, R. and Reeves, C.M., "Function Minimization by Conjugate Gradients," *Computer Journal*, Vol. 7, April 1964, pp. 149-154.

[16] Rosenhead, L., *Laminar Boundary Layers*, Oxford, 1963, pp. 540-544.

[17] Scruggs, R.M., Nash, J.F., and Singleton, R.E., "Analysis of Dynamic Stall Using Unsteady Boundary-Layer Theory," NASA CR-2462, Oct. 1974.

[18] Cebeci, T., Mosinskis, G.J., and Smith, A.M.O., "Calculation of Separation Points in Incompressible Turbulent Flows," *Journal of Aircraft*, Vol. 9, Sept. 1972, pp. 618-624.

[19] Knutsen, R.W., "Two-Dimensional and Axisymmetric Boundary-Layer Analysis, Program TEA-200," Boeing Document D6-29343 TN, Seattle, Wash., 1970.

[20] Abbott, I.H., "Lift, Drag and Pressure-Distribution Tests of Six Airfoil Models Submitted by Consolidated Aircraft Corporation as Sections of a Wing for the XB-36 Airplane," NACA MR-612, Feb. 18, 1942.

[21] Kinsey, D.W. and Bowers, D.L., "Computerized Procedure to Obtain the Coordinates and Section Characteristics of NACA Designated Airfoils," Air Force Flight Dynamics Lab., Wright-Patterson AFB, Ohio, AFFDL-TR-71-87, Nov. 1971.

[22] Abbott, I.H., von Doenhoff, A.E., and Stivers, L.S., "Summary of Airfoil Data," NACA Rept. 824, 1945.

[23] Beasley, W.D. and McGhee, R.J., "Experimental and Theoretical Low-Speed Aerodynamic Characteristics of the NACA $65_1$-213, $a = 0.50$, Airfoil," NASA TM X-3160, Feb. 1975.

[24] Stivers, L.S., "Effects of Subsonic Mach Numbers on the Forces and Pressure Distributions on Four NACA 64A-Series Airfoil Sections at Angles of Attack as High as 28°, NACA TN 3162, Mar. 1954.

[25] Tetervin, N., "Test in the NACA Two-Dimensional Low-Turbulence Tunnel of Airfoil Sections Designed to Have Small Pitching Moments and High Lift-Drag Ratios," NACA WR L-452, (CB 31 13, Sept. 1943).

[26] Townsend, A.A., "The Behaviour of a Turbulent Boundary-Layer Near Separation," *Journal of Fluid Mechanics*, Vol. 12, Pt. 4, April 1962, pp. 536-554.